A Zwitterionic Hydrogel#Based Heterogeneous Fenton Catalyst for Water Treatment

RESEARCH ARTICLE

NANO · MICRO small
www.small-journal.com

A Zwitterionic Hydrogel-Based Heterogeneous Fenton Catalyst for Water Treatment

*Devashish Gokhale, Ian Chen, Wan-Ni Wu, Arthur Monne Gagnaire, and Patrick S. Doyle**

Persistent organic pollutants (POPs), including xenoestrogens and polyfluoroalkyl substances (PFAS), demand urgent global intervention. Fenton oxidation, catalyzed by iron ions, offers a cost-effective means to degrade POPs. However, numerous challenges like acid dependency, catalyst loss, and toxic waste generation hinder practical application. Efforts to create long-lasting heterogeneous Fenton catalysts, capable of simultaneously eliminating acid requirements, sustaining rapid kinetics, and retaining iron efficiently, have been unsuccessful. This study introduces an innovative heterogeneous zwitterionic hydrogel-based Fenton catalyst, surmounting these challenges in a cost-effective and scalable manner. The hydrogel, hosting individually complexed iron ions in a porous scaffold, exhibits substantial effective surface area and kinetics akin to homogeneous Fenton reactions. Complexed ions within the hydrogel can initiate Fenton degradation at neutral pH, eliminating acid additions. Simultaneously, the zwitterionic hydrogel scaffold, chosen for its resistance to Fenton oxidation, forms strong bonds with iron ions, enabling prolonged reuse. Diverging from existing designs, the catalyst proves compatible with UV-Fenton processes and achieves rapid self-regeneration during operation, offering a promising solution for the efficient and scalable degradation of POPs. The study underscores the efficacy of the approach by demonstrating the swift degradation of three significant contaminants—xenoestrogens, pesticides, and PFAS—across multiple cycles at trace concentrations.

1. Introduction

Persistent organic pollutants (POPs) are organic pollutants that undergo natural degradation in the environment only over several years or decades. POPs include chemically diverse materials such as organic solvents, chemical intermediates, industrial surfactants, lubricants, detergents, disinfectants, antibiotics and other medications, food additives and flavoring agents.[1,2] Though they typically occur at low concentrations (μ g L^{-1}), the tendency of POPs to accumulate inside the body and the environment over these long time scales makes them subjects of significant environmental concern. POPs are ubiquitous in the environment[3,4] and can have significant adverse effects on the ecosystem (including cancer in humans and animals, and the increased prevalence of antibiotic-resistant diseases).[5–12] Although the Stockholm Convention on Persistent Organic Pollutants imposed global restrictions on the manufacture and use of specific POPs, these still persist in the environment where they continue to have negative impacts on the ecosystem, and are expected to do so for several decades.[13,14] At the same time, newer "designer" POPs continue to be manufactured, sometimes as industrial substitutes for restricted substances.[15] Among other POPs, the US Environmental Protection Agency (USEPA) and the European Chemicals Agency (ECHA) are currently in the process of imposing ever-stricter limits on polyfluoroalkyl substances (PFAS) in the environment,[16,17] increasing the urgency of the need for technologies to remove POPs from water. Such technologies will also be essential to meet the targets of United Nations Sustainable Development Goal (UNSDG) 6.[18]

Addressing the POP problem requires a combination of techniques for the sequestration and destruction of POP molecules, and is made challenging by the chemical diversity and stability of POPs.[19] Destructive methods are necessary to accelerate the slow natural degradation of POPs in water and waste streams, including those in concentrated streams produced by traditional sequestration technologies like reverse osmosis or activated carbon adsorption, and are an essential part of the solution to the POP problem. In this context, various advanced oxidation processes (AOPs) using ozone or hydrogen peroxide in

D. Gokhale, W.-N. Wu, A. Monne Gagnaire, P. S. Doyle
Department of Chemical Engineering
Massachusetts Institute of Technology
77 Massachusetts Avenue, Cambridge, MA 02139, USA
E-mail: PDOYLE@MIT.EDU
I. Chen
Department of Materials Science and Engineering
Massachusetts Institute of Technology
77 Massachusetts Avenue, Cambridge, MA 02139, USA
A. Monne Gagnaire
Department of Chemistry and Applied Biosciences
Eidgenössische Technische Hochschule (ETH-Zürich)
Zürich 8093, Switzerland

The ORCID identification number(s) for the author(s) of this article can be found under https://doi.org/10.1002/smll.202402525

DOI: 10.1002/smll.202402525

combination with a catalyst to produce highly reactive hydroxyl radicals to attack POPs in situ have been developed. One of the most well-known AOPs today, the Fenton reaction, uses Fe(II) ions as the underlying catalyst.[20] The Fenton reaction, shown in Equation (1), has found substantial interest in academia and industry due to its ability to destroy chemically diverse POPs efficiently, including those known to be difficult to degrade using other AOPs.[21–25] The low cost of materials required to implement the process also makes Fenton AOPs promising for use in real world scenarios.[26,27]

$$Fe^{2+} + H_2O_2 \xrightarrow{H+} Fe^{3+} + OH^- + OH^{\bullet} \quad (1)$$

Equation (1) summarizes the overall Fenton reaction, which is composed of numerous elementary steps, some of which are still an active area of study, and controlled by a combination of the kinetics of these steps and mass transfer effects.[28] It must be noted, as shown in Equation (1), that the Fe(II) ions in a classical Fenton reaction are not true catalysts since they are continuously converted into Fe(III) ions that have a limited ability to degrade contaminants. Further, the Fe(II) ions are dissolved in the water to be treated, so subsequent separation steps are necessary to eliminate the iron and obtain clean water.[29,30] Due to the presence of other contaminants, formation of sludge, and considerations of cost, any recovered iron is disposed of as toxic chemical waste and cannot be reused.[31,32] Fenton oxidation optimally occurs at a pH close to 3.0, necessitating acid addition to degrade POPs on the short timescales encountered in real-world water treatment processes, significantly adding to process complexity and cost.[25,33] A treatment process based on the classical Fenton reaction typically requires at least four unit operations with multiple pumps, sensors, and controls, alongside continuous acid, iron, hydrogen peroxide, and base addition (for neutralizing acids).[29,30] In order to operate a more practical and cost-effective process based on the Fenton reaction, it is necessary to retain and reuse the iron within the unit operation by immobilizing it in a heterogeneous catalyst, while also eliminating the need to add acid.

Previous attempts to retain iron have included preparing iron or iron oxide nanoparticles that are immobilized on a traditional adsorbent like activated carbon,[34,35] other substrates,[36,37] or inside a polymer such as chitosan.[38] Adding acid to such a system is still necessary to achieve rapid Fenton oxidation, but acid addition can dissolve nanoparticles and significantly reduces catalyst life. Reaction kinetics are significantly slowed in the absence of acid addition (due to the increase in Fe(III) ions relative to Fe(II) ions, Fe(III) ions reacting much more slowly), or if nanoparticles are replaced with bulk iron or iron oxide (due to reduction in active surface area).[23,24] Current approaches to retain iron are therefore not amenable to the elimination of acid addition.

On the other hand, approaches to eliminate acid addition while maintaining rapid kinetics focus on preparing soluble complexes of iron, in which the ligands are necessary to produce reactive hydroxyl radicals at higher pH.[39–41] The increased production of hydroxyl radicals may be attributed to a change in the effective work function of the iron, in accordance with the Haber–Weiss mechanism.[42] Since these complexes are water-soluble, it is not possible to effectively retain the iron. Iron complexes also face two further limitations: 1) the ligands are often subject to degradation due to Fenton oxidation, limiting longevity, and 2) changes in the oxidation state of the iron ions during the Fenton reaction can cause unstable complexes to fall apart, releasing the bound iron.[43,44] Current approaches to eliminate acid addition are therefore not amenable to iron retention.

There are also additional challenges associated with current approaches; primarily, Fenton oxidation degrades not only the target POPs, but also many of the encapsulating polymers, ligands, and associated substrates that are used to improve the classical Fenton reaction.[38,43,45,46] In general, AOP performance may be further boosted by the simultaneous use of ultraviolet (UV) light, which can degrade molecules directly (photolysis) or by accelerating the production of hydroxyl radicals from hydrogen peroxide to degrade POPs.[47] Although UV–Fenton processes have been explored and show great promise for POP elimination, they make the design of a heterogeneous catalyst more challenging, requiring it to be transparent, and any complexing ligand to be UV resistant.[23,24]

In sum, a practical and efficient Fenton process to eliminate POPs requires the development of 1) a heterogeneous catalyst that retains iron while 2) eliminating the need for acid addition, 3) is highly porous and has a large effective surface area to preserve efficacy, 4) is optically transparent and 5) resistant to degradation by UV light, hydrogen peroxide, and the Fenton reaction itself, 6) preferably does not use nanoparticles that may pose a threat to the environment if they escape the catalyst, and 7) can be regenerated rapidly and reused in a facile way. Combining the use of zwitterionic hydrogels for water treatment with ideas from single-atom catalysis, this work introduces a zwitterionic hydrogel catalyst containing chelated iron to simultaneously satisfy all these criteria. The practical efficacy of the catalyst is demonstrated by showcasing the degradation of ethinyl estradiol (EDOL; a xenoestrogen), perfluorooctanoic acid (PFOA; a model for PFAS, fluorinated POPs and industrial surfactants), and 2,4-dichlorophenol (DCP; a model for pesticides and chlorinated aromatics). All three molecules are of significant global concern and there is an urgent need for strategies to eliminate each of them.[48]

Hydrogels have previously been used to immobilize other enzymatic catalysts.[49] Simultaneously, there is significant interest in applying hydrogels to solve problems in water treatment due to the several unique advantages they offer.[19,50–52] First, hydrogels can be prepared from a vast library of mutually compatible and commercially available molecules, allowing the facile design of structures with specific functional groups and chemical properties. Chemical flexibility allows us to create a polymeric hydrogel structure containing ligand-like groups that can bind individual iron ions to hold them within the gel, while simultaneously changing the work function of iron ions to enable Fenton oxidation at neutral pH. As we show in this work, appropriate precursor materials can be used to prepare hydrogels that are optically transparent and resist oxidation. Further, the affinity of hydrogel backbones to water and their tendency to swell when wet leads to architectures with high microporosity and water content, facilitating the passage of contaminants into hydrogel structures. In prior work, we used functionalized hydrogels to absorb contaminants from water by leveraging these features to prepare materials that exhibited high mass transfer coefficients and imposed minimal transport limitations on contaminant molecules.[19,52]

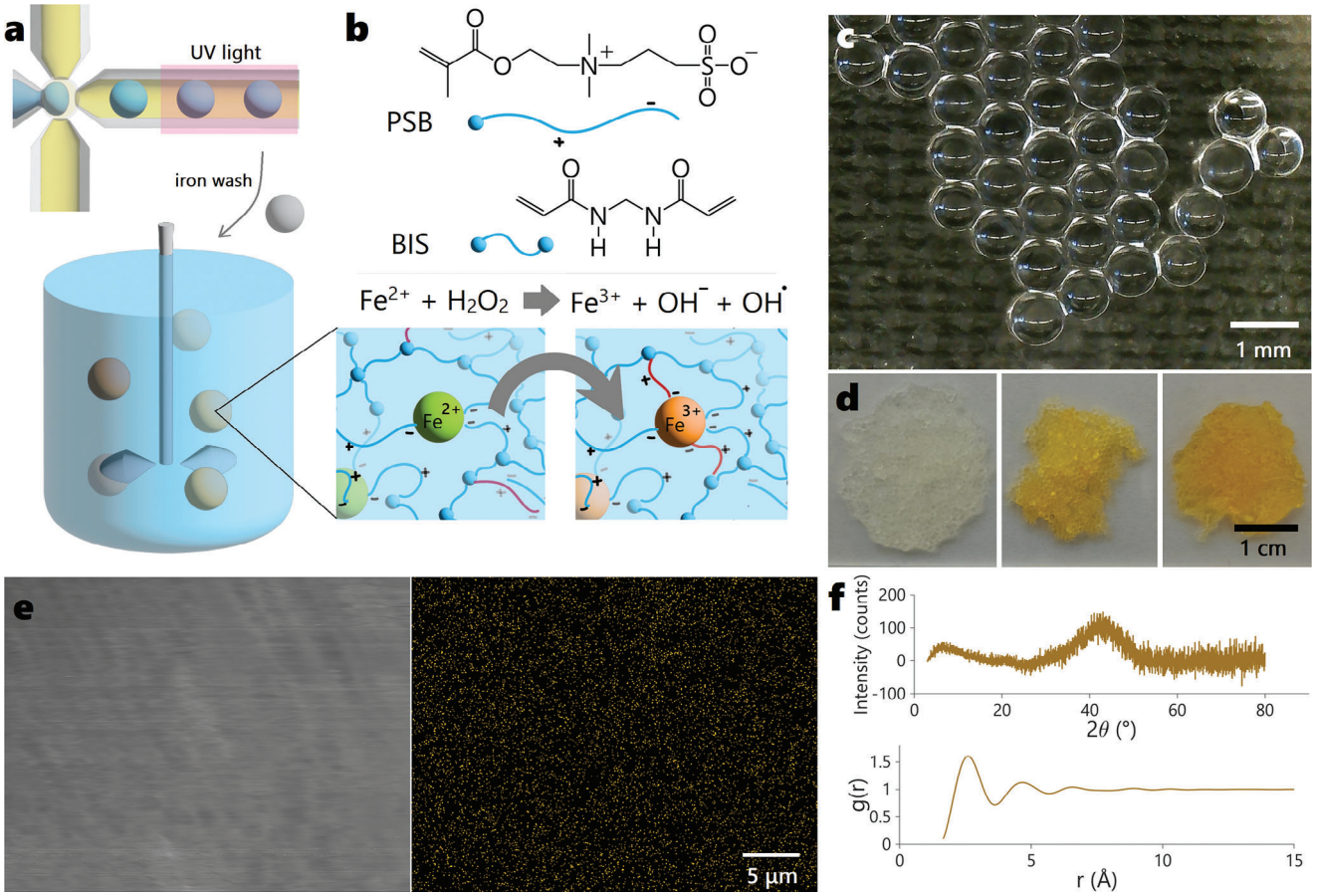

Figure 1. Synthesis and characterization of iron-functionalized zwitterionic hydrogel microparticles. a) A monomer solution (blue) is pinched off using mineral oil (yellow) to prepare droplets in an off-the-shelf microfluidic device. Droplets are photo-polymerized into microparticles using UV light and soaked in iron to functionalize them, and can subsequently be used to catalyze Fenton oxidation in a stirred tank. b) The hydrogel microparticles are constructed using a zwitterionic monomer (PSB) and crosslinker (BIS). c) Microparticles prepared using this method are optically transparent and 800 ± 100 µm in size. d) Clear microparticles obtained after polymerization (left) become yellow after iron functionalization (center), and dark orange after being used to catalyze Fenton oxidation in the absence of UV light (right). e) An scanning electron microscopy (SEM) micrograph and corresponding energy dispersive X-ray spectroscopy (EDS) map of iron, showing uniform distribution. f) An X-ray diffraction (XRD) spectrum (top) obtained from the iron-functionalized microparticles, and the pair correlation function g(r) obtained therefrom (bottom).

The inherent kinetic advantages of binding individual iron ions (rather than nanoparticles), combined with rapid mass transport, makes hydrogels ideal scaffolds for supporting fast POP degradation. The synthesis of the hydrogel catalyst is a facile and scalable process, requiring off-the-shelf equipment that operates at room temperature and does not use hazardous chemicals. Finally, we show that a catalyst structured in this manner and operated in a UV–Fenton process can continuously regenerate itself and be reused, without the need for any additional processing, making our catalysts promising solutions to degrade POPs.

2. Results and Discussion

2.1. Strategy and Synthesis

Hydrogels are synthesized from monomer solutions as described in the Experimental Section, and shown in **Figure 1a**. The catalyst synthesis is facile, occurs at ambient conditions, and is highly scalable. In brief, we begin with a monomer solution consisting of precursors shown in Figure 1b and a photoinitiator (PI) dissolved in water. The monomer solution is processed into monodisperse droplets using an off-the-shelf microfluidic device (micro-cross) that operates by pinching off the monomer solution using an immiscible mineral oil phase (Figure 1a). There are well-known methods of scaling up the production of these devices, to produce large quantities of hydrogels for commercial use.[53] The droplets are then exposed to UV light, triggering the formation of free-radicals from the PI molecules. These free-radicals attack the terminal double bonds in the hydrogel precursor molecules in a chain-growth polymerization reaction that converts the droplets into solid hydrogel microparticles containing water (see Figure S1, Supporting Information). A picture of these hydrogel microparticles, washed with water after synthesis to remove unreacted molecules, is shown in Figure 1c. The microparticles have a uniform size of 800 ± 100 µm, which is large enough to separate them from water by simple gravitational settling for a few seconds (to enable retention within a unit operation without additional separation steps), but small enough to

limit the length scales on which POP molecules need to be transported inside the hydrogel, leading to faster kinetics. Creating hydrogels in the form of microparticles also enables us to limit the extinction of UV light as it passes through and is absorbed by the hydrogels in a UV–Fenton process.

Using (2-(Methacryloyloxy)ethyl)dimethyl-(3-sulfopropyl)ammonium hydroxide (PSB) and N,N'-methylenebis(acrylamide) (BIS) as the hydrogel precursors allows several advantages. PSB forms the bulk of the hydrogel, while BIS acts to cross-link PSB chains and stabilize the entire structure. Hydrogel microparticles prepared using this method are mechanically robust (see Supporting Information 2.1 and Figure S2, Supporting Information). At the same time, PSB also contains charged groups (Figure 1b) that make it superhydrophilic,[19] increase its solubility, and limit polymerization-induced phase separation (PIPS) during the synthesis process. As such, microparticles made from PSB are internally homogeneous and have a very high water content, making them optically transparent to support the passage of UV light (Figure 1c and Figure S3, Supporting Information). The superhydrophilicity of PSB hydrogels leads to greater swelling than other conventional hydrogels, increasing mesh size and increasing the rate of POP transport (see Supporting Information 1.1 and 1.2). Although the hydrogel is swollen, the negatively charged terminal oxygen atoms on the PSB molecule serve to strongly bind Fe(II) and Fe(III) ions through the formation of coordinate bonds.[19] As such, the hydrogel microparticles can be made to bind Fe(II) ions simply by soaking them in a saturated solution of ferrous sulfate as described in the Experimental Section. Finally, a synthesis based on PSB does not consume any hazardous chemicals, and since we leave the bound iron ions in a solvated state (rather than sintering, as in other catalysts), the entire process can be operated at room temperature.

The presence of bound iron within the microparticles may be confirmed by visual inspection, after the soaked microparticles are washed extensively with water to remove any free iron ions. As shown in Figure 1d, the once clear microparticles are seen to turn yellow after being used to bind iron. Though Fe(II) ions are blue-green, the microparticles look yellow due to a combination of 1) a changed work-function due to the formation of coordinate bonds, affecting the absorbance spectrum of the ions, and 2) the formation of trace quantities of yellow-brown Fe(III) ions due to exposure to atmospheric oxygen. The hydrogel microparticles containing bound iron may then be used to catalyze Fenton oxidation as shown in Figure 1a, with Fe(II) ions within the hydrogel being oxidized to Fe(III) ions while hydrogen peroxide is converted to hydroxyl radicals. The absence of UV light and using limited quantities of hydrogen peroxide suppress reverse reactions that convert Fe(III) ions to Fe(II) ions,[21,47] and the microparticles can be seen to change color from yellow to orange-brown as the relative concentration of Fe(III) ions increases (Figure 1d).

To maximize the rate of Fenton oxidation, the loading of iron ions within the hydrogel microparticles should be maximized, and these ions should be well-dispersed within the hydrogel to increase the effective surface area of the reaction. Soaking the hydrogels microparticles in a saturated solution of ferrous sulfate enables us to achieve an internal iron concentration of 0.023% (w/w) or 233 ppm (parts-per-million), determined using thermogravimetric analysis (see Supporting Information 2.3 and Figure S4, Supporting Information). Classical homogeneous Fenton reactions effective in degrading POPs have been reported in literature with iron concentrations as low as 0.1μM or 0.0005% (w/w), which is two orders of magnitude lower than within our microparticles,[40] so the local concentration of iron ions within the hydrogel microparticles is sufficient to drive Fenton oxidation. Further, iron ions avoid forming clusters within the hydrogel due to the presence of repelling positive charges on each ion. The absence of clusters is confirmed using elemental mapping (SEM-EDS, Figure 1e), indicating the absence of clusters at the μm scale, and using X-ray diffraction (XRD) to study clustering at the nm scale (Figure 1f). The XRD spectrum of microparticles containing bound iron is assumed to capture information solely about iron–iron correlations due to the significantly larger form factor of iron ions compared to other elements in the hydrogel.[54] The absence of sharp or tall peaks in the XRD spectrum indicates an amorphous distribution with crystallites, if any, being smaller than 120 ions in size (Supporting Information 2.4). As also described in Supporting Information 2.4, the XRD spectrum may be used to calculate a pair correlation function indicating the spatial distribution of ions relative to each other (Figure 1f). The pair correlation function has a characteristic liquid-like shape, indicating that the iron ions are well-dispersed inside the hydrogel.

As a result of these design choices, hydrogel microparticles containing bound iron ions are able to catalyze the Fenton degradation of organic molecules on time scales similar to classical Fenton degradation by free iron ions in water. **Figure 2**a shows the degradation of methylene blue dye in a batch experiment using catalytic hydrogel microparticles that have a total mass approximately one-tenth that of the solution (see Experimental Section). Methylene blue is a model organic pollutant commonly used in literature to study the efficacy of Fenton degradation.[55–58] The concentrations of methylene blue dye and hydrogen peroxide, and the effective concentration of iron (per volume of solution to be treated) used here are at the lower end of the concentration range examined in these prior works, and are therefore suitable benchmark conditions to study the performance our catalyst. These overall concentrations are kept constant when comparing catalytic hydrogel microparticles to free iron. Interestingly, the hydrogel microparticles were able to catalyze dye degradation at low concentrations, and at neutral pH in the absence of added acid. Here, our hydrogels serve not only to bind iron ions, but also act as ligands to change work function (as in prior work[39–41,43]) and enable Fenton oxidation at higher pH. Dye degradation was rapid and complete in 10 s. We track the progress of the reaction by measuring the hue of a representative cross-section described in the Experimental Section. The rate of dye degradation for a neutral pH process catalyzed by hydrogel microparticles are compared to a classical Fenton process at pH 3.0 using the same quantity of dissolved iron (Figure 2b). In control experiments, we verified that the classical Fenton process was unable to degrade methylene blue in the absence of acid or hydrogen peroxide addition (see Figure S5, Supporting Information), implying that the hydrogel scaffold helps enhance the rate of hydroxyl radical formation at high pH. These dye degradation data can be used to calculate first-order time constants that have the same order of magnitude (2.54 s for hydrogel-chelated iron, and 0.82s for free iron in a classical Fenton process). It must be

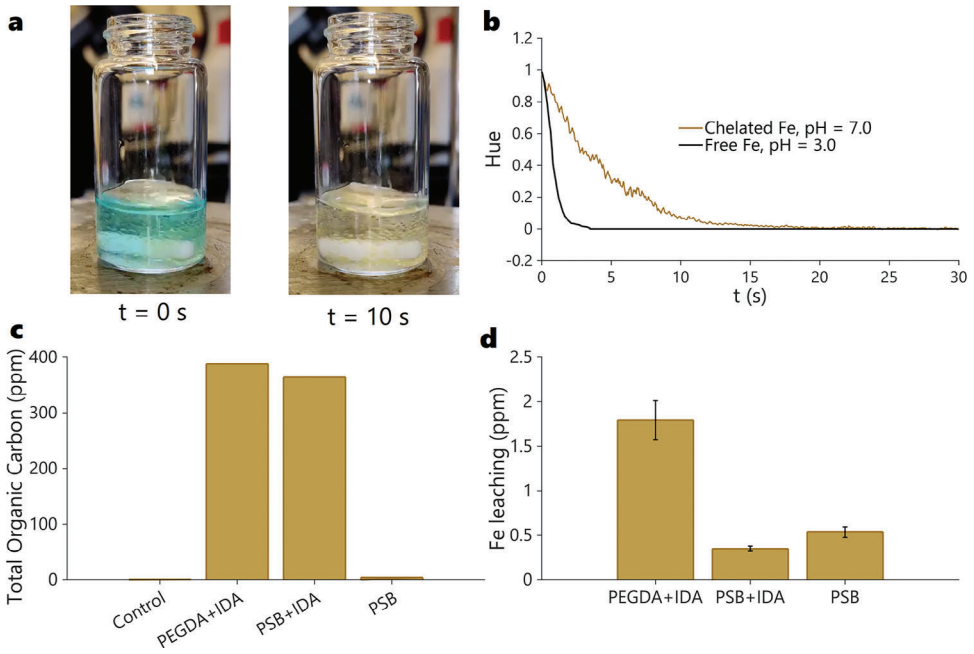

Figure 2. Effect of binding iron within a zwitterionic hydrogel on Fenton kinetics and catalyst life. a) Images before and after the rapid degradation of methylene blue dye in a stirred vial containing hydrogel microparticles at neutral pH. b) The kinetics of the process in (a) compared to the same process with an equal concentration of free iron ions in solution at pH 3.0, measured as the change in the hue of the solution over time. c) The total organic carbon (TOC) content in water obtained after a Fenton reaction in the absence of POPs is catalyzed by three different iron-functionalized hydrogels. d) The concentration of iron measured in the supernatant after the reactions described in (c). Error bars represent one standard deviation (n=3).

noted that these time constants are controlled by mass transfer and not reaction kinetics,[28] and the comparable performance of hydrogel-chelated iron and free iron imply a lack of significant reduction in mass transfer due to the introduction of a hydrogel scaffold. The rapid transport of organic molecules through hydrogel microparticles has been noted in prior work, and is one of the key advantages of using hydrogels to prepare such scaffolds.[19]

The hydrogel catalyst produces highly reactive hydroxyl radicals to degrade dyes and other contaminants. These same radicals may attack the hydrogel scaffold.[38] As such, it is important to pick a hydrogel chemistry that is resistant to degradation. Previous attempts at Fenton catalysts that function at neutral pH (via the use of ligands) are susceptible to this failure mode, due to ligand degradation.[43] We measure TOC content produced by three types of iron-laden hydrogel catalysts (PEGDA-IDA, PSB-IDA, and PSB) in the reaction medium at the end of a day-long experiment that exactly mimics those shown below to degrade POPs, except for the lack of a POP and larger quantity of hydrogel to aid quantification. These data are obtained as described in the experimental section and shown in Figure 2c. The first hydrogel material, polyethylene glycol diacrylate (PEGDA), is a commonly used model for hydrogel biomaterials, and is used here to illustrate this lack of degradation resistance typically observed with these materials. Since PEGDA does not have sites to bind iron to create a catalyst which may be compared with our (PSB) catalyst, we copolymerize it with a functionalized chelating agent, iminodiacetic acid (IDA) to increase the iron loading.[19] IDA is the functional basis of numerous commercial ion-exchange resins, so degradation of a PEGDA-IDA scaffold not only demonstrates the susceptibility of traditional hydrogel scaffolds to be degraded as in prior work,[38] but also of commercial ion exchange resins (which are natural choices for materials to load with well-dispersed iron to catalyze Fenton reactions). However, it is important to isolate degradation due to the hydrogel scaffold from degradation due to the chelating agent used to bind iron. Therefore, we tested a second hydrogel, PSB-IDA. The PSB-IDA hydrogel also undergoes degradation, but to a lesser extent, indicating the importance of the hydrogel backbone, but also the greater dependence of scaffold stability on the chemistry that locally surrounds the iron ions. Finally, our scaffold material, PSB is tested and compared to these previous hydrogels, demonstrating its stability in the highly oxidative conditions of the Fenton reaction (degradation is <0.005% by mass). In Supporting Information 1.3, we carefully review literature to examine the effect of Fenton degradation on polymers to identify two heuristics that seem to select for polymer stability: 1) the absence of heteroatoms or polar bonds along the polymer backbone, and 2) the presence of electron-withdrawing side groups on the polymer chain. The PSB scaffold fulfils both criteria since 1) the polymer backbone, being a polyacrylate, has only carbon atoms along the backbone (Figure S1, Supporting Information), and 2) the sulfobetaine side-group contains electron-withdrawing ester and ammonium moeieties close to the polymer backbone (Figure 1b).

In addition to structural stability, strong chemical bonds between the hydrogel and iron ions are necessary to retain iron. Previous attempts at heterogeneous Fenton catalysts using iron nanoparticles that are operated at acidic pH are susceptible to this failure mode, as acidic pH causes the dissolution of iron into water.[59] Figure 2d shows the amount of iron released from iron-laden hydrogels when they are used to catalyze UV–Fenton

reactions in the absence of POPs. It must be noted that these values, measured using inductively coupled plasma-mass spectrometry (ICP-MS) analysis as described in the experimental section, only capture dissolved iron, and not the loss of iron that remains associated to large residues (>200 nm) produced by hydrogel degradation described in Figure 2c. From Figure 2d, it may be noted that PSB-containing hydrogels, which possess a large number of moeities to bind iron (see Supporting Information 1.4) as a result of negatively charged oxygen atoms in Figure 1b, have a greater affinity for iron than classical hydrogel materials. This greater affinity, combined with the higher affinity of PSB-IDA hydrogels to bind iron is consistent with prior work that used these hydrogels as absorbents to remove metals from water.[19] Finally, the loss of iron from iron-laden PSB hydrogels per 24 h UV–Fenton cycle is 0.013 mg g^{-1} of hydrogel, or 2.1% of the total amount of retained iron, indicating that the substantial majority of iron is effectively retained within the catalyst. When implemented as a continuous process with 10% (w/w) hydrogel in water and a 10 min residence time, the concentration of iron in the treated stream will be 0.1 ppm, well below the USEPA drinking water secondary maximum contaminant level (MCL), implying that no secondary treatment is needed before the water is used for human consumption or released into the environment.[60] The inherent flexibility of chains within the hydrogel enable the motion of PSB chains to bind to or unbind from iron ions bound to the hydrogel even as the iron ions undergo oxidative or reductive changes (shown using red PSB molecules in Figure 1a), enabling significant iron retention during the Fenton reaction. When operating at scale for extended durations, iron content can occasionally be replenished by washing with a saturated iron(II) solution. Given the small amount of iron needed, the same regenerant can be reused multiple times. However, we do not replenish iron in our lab-scale experiments. Subsequent data further support the longevity of the hydrogel catalyst suggested by these TOC and iron leaching data.

2.2. POP Elimination Kinetics and Reusability

We use catalytic hydrogel microparticles to showcase the destruction of three model POPs of significant environmental concern (EDOL, DCP, and PFOA) whose structures are shown in **Figure 3a**. Prior work that uses Fenton reactions has demonstrated the successful degradation of these molecules.[61–63] It is important to demonstrate the degradation of small molecule POPs such as these on practical time scales and at environmentally relevant concentrations, since the degradation of dyes is accelerated by electron-transfer effects.[64] PSB hydrogel microparticles containing chelated iron ions are able to effectively eliminate these recalcitrant POPs by catalyzing a UV–Fenton batch process in a stirred vessel continuously exposed to UV light as described in the experimental section. The initial POP concentration is 1 ppm, and sufficient hydrogen peroxide is added at the beginning of the reaction to yield an initial concentration of 0.07% (w/w). Final POP concentrations are measured after 24 h using liquid chromatography–mass spectroscopy (LC–MS) as described in the Experimental Section (also see Supporting Information 2.5), and indicate complete elimination of EDOL and DCP, and significant elimination of PFOA. PFOA elimination can be increased in real-world water treatment processes by operating multiple batch units (such as the ones described in this work) sequentially, or by the continuous addition of hydrogen peroxide into a single unit in continuous operation. The elimination achieved using our heterogeneous UV–Fenton process is similar to elimination observed in prior work,[61–63] and demonstrates the ability of our catalytic hydrogel microparticles to degrade POPs at trace levels.

We choose to operate our Fenton process in the presence of UV light due to the faster and higher equilibrium elimination achieved in the UV–Fenton process compared to a Fenton process without UV light, the activation of hydrogen peroxide by UV light, or solely by the action of UV light or absorption (shown for EDOL in Figure 3b). We verified that the degradation of all model POPs was due to the UV–Fenton process, and not simply due to the presence of UV light (also see Figure S6, Supporting Information), as has been reported in prior work.[47] It should be noted that the UV light used in these studies is in the UVA spectrum (365 nm), and not the deep-UV that is more energy intensive and sometimes used in literature to degrade POPs.[65] The overall rate of UV–Fenton degradation is also dependent on the initial concentration of the POP to be degraded. As shown in Figure 3c, we observed that lowering the initial POP concentration increased the fractional elimination at equilibrium but reduced the speed of elimination. Since the initial concentration of hydrogen peroxide, bound iron, and the intensity of UV light were kept constant in these experiments, it may be assumed that the UV–Fenton reaction that produces hydroxyl radicals (Figure 1a) does so at a rate that is identical over time across all three systems in Figure 3c. As such, the concentration of hydroxyl radicals is independent of the initial POP concentration over time. As we lower the POP concentration, the number of hydroxyl radicals relative to the number of POP molecules increases, leading to an increase in equilibrium elimination. However, since the POP molecules have a lower concentration, the kinetics of the degradation reactions are slower, leading to a decrease in the rate of elimination.

The rate of UV–Fenton degradation and equilibrium elimination also depend on the initial concentration of hydrogen peroxide loaded into the reaction mixture, as shown in Figure 3d–f. Interestingly, the data show that POP degradation first increases and then decreases as the initial concentration of hydrogen peroxide is increased. For PFOA, it is as important to defluorinate the reaction by-products as it is to degrade the target molecule for environmental applications. We measure the defluorination of PFOA as a function of initial hydrogen peroxide concentration using ion chromatography experiments, observing the same non-linear trend (see Supporting Information 2.6 and Figure S7, Supporting Information). Although this effect has not been observed in classical Fenton degradation experiments, it has previously been reported in heterogeneous Fenton degradation experiments.[66,67] As the concentration of hydrogen peroxide increases, the rate of production of hydroxyl radicals close to the iron ions within the hydrogels also increases. These hydroxyl radicals then diffuse outward and react with POP molecules that are continuously diffusing into the hydrogel microparticles, thereby degrading the POP. However, as shown in prior work,[66,67] when the initial concentration of hydrogen peroxide

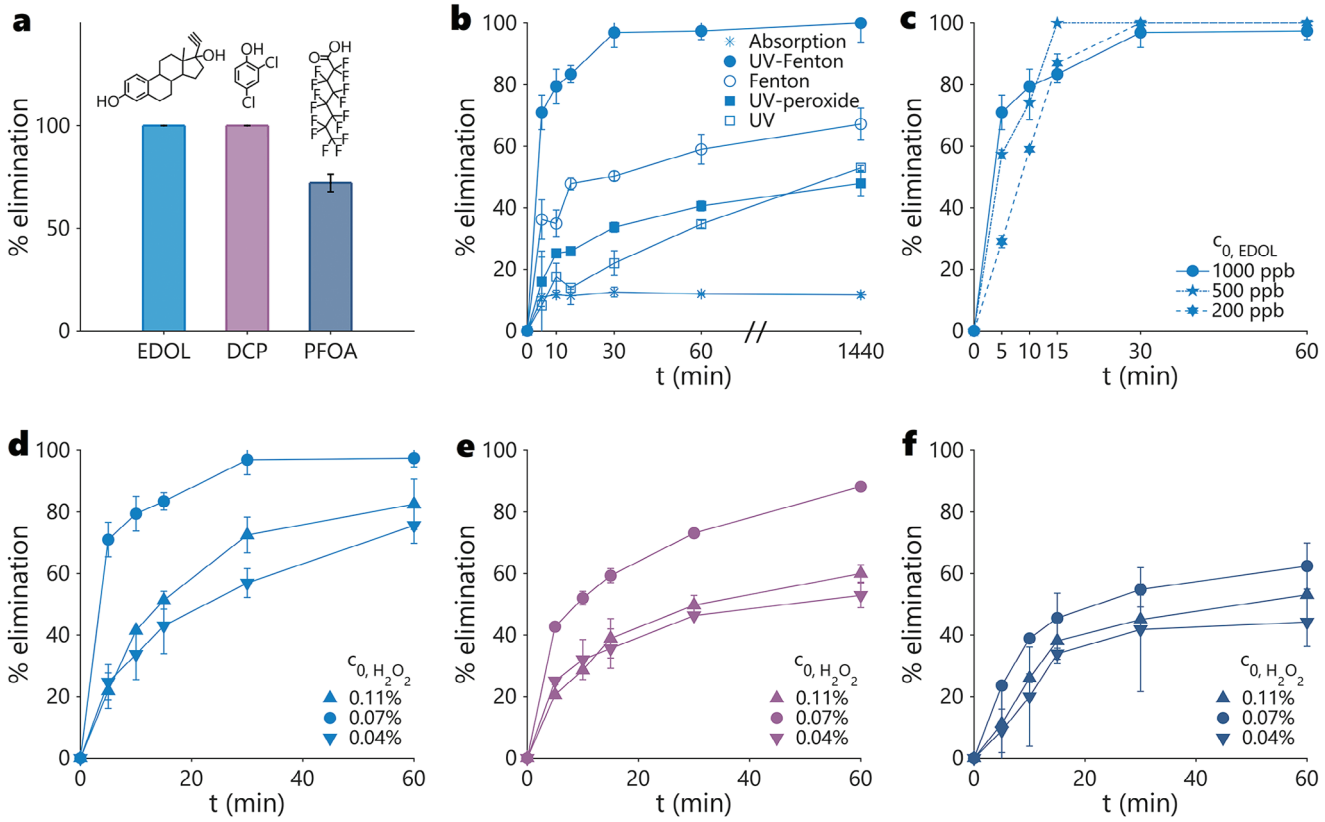

Figure 3. Rate and extent of elimination of model POPs in batch processes at environmentally relevant concentrations. a) Structures and elimination of three model POPs at equilibrium. b) Rate and equilibrium elimination of EDOL by UV light, by absorption into the hydrogel microparticles, by the effect of UV light and hydrogen peroxide in the absence of hydrogel microparticles, by the classical Fenton reaction using hydrogel microparticles, and by the UV–Fenton reaction using hydrogel microparticles, for an initial EDOL concentration of 1000 parts-per-billion (ppb) and initial hydrogen peroxide concentration of 0.07% (w/w). c) Rate and equilibrium elimination of EDOL with varying initial concentration, using the same amount of hydrogen peroxide and iron-functionalized hydrogel (0.02 g mL^{-1}). d–f) Rate and equilibrium elimination of d) EDOL, e) DCP, and f) PFOA, with varying initial hydrogen peroxide concentration, with initial POP concentration of 1000 ppb. All experiments are performed twice and data are measured thrice. Error bars are one standard deviation.

is increased beyond a critical value, the concentration of hydroxyl radicals close to the catalytic sites (here, the iron ions) increases sufficiently that reactions between hydrogen peroxide molecules and the hydroxyl radicals to produce hydroperoxy radicals occur faster than the outward diffusion of hydroxyl radicals. These radicals have the same capacity to degrade POPs as hydroxyl radicals, but require greater quantities of hydrogen peroxide to make. As such, the normalized degradation capacity of each hydrogen peroxide molecule is reduced, and POP degradation decreases above the critical threshold of initial hydrogen peroxide concentration. The value of this threshold is set by competition between the mass transport of hydroxyl radicals (affected by the size of the hydrogel microparticles and mixing within the reaction setup) and the rate of formation of hydroperoxy radicals (affected by the concentration of hydrogen peroxide, bound iron, and the intensity of UV light), and is therefore independent of the POP being degraded (Figure 3d–f).

Regenerating Fenton catalyts requires the use of the reverse-Fenton reactions shown in **Figure** 4a, which have been extensively explored in literature.[47] In commercial classical Fenton processes, it is not possible to regenerate and reuse the catalyst because: 1) the catalyst is not retained separately from the water to be treated, requiring additional separation steps to recover the iron, adding significant cost; 2) Fe(III) ions have a tendency to form a sludge if the pH is not tightly controlled to be between 3.0 and 4.0;[68] 3) the reverse Fenton reactions are suppressed by the presence of excess protons in these acidic environments; 4) the reverse-Fenton reactions proceed two to three orders of magnitude more slowly than the forward Fenton reaction in the absence of UV light.[21] Our materials overcome these challenges due to their innate ability to strongly bind and retain iron, and to operate at neutral pH as described in previous sections. Further, if the catalytic microparticles are used in a UV–Fenton process to accelerate POP degradation (Figure 3b), the same UV light can drive the reverse-Fenton reactions simultaneously with the forward Fenton reaction. As shown in Figure 4a, the simultaneity of the forward and reverse Fenton reactions obviates the need for a separate regeneration step, and catalytic hydrogel microparticles may continuously be reused as long as fresh hydrogen peroxide is added to drive reactions in both directions. As an aside, the reverse-Fenton reactions also produce hydroxyl radicals that can attack POPs,[69–71] and are one of the reasons why the UV–Fenton process is more effective than the Fenton process without UV (Figure 3b).

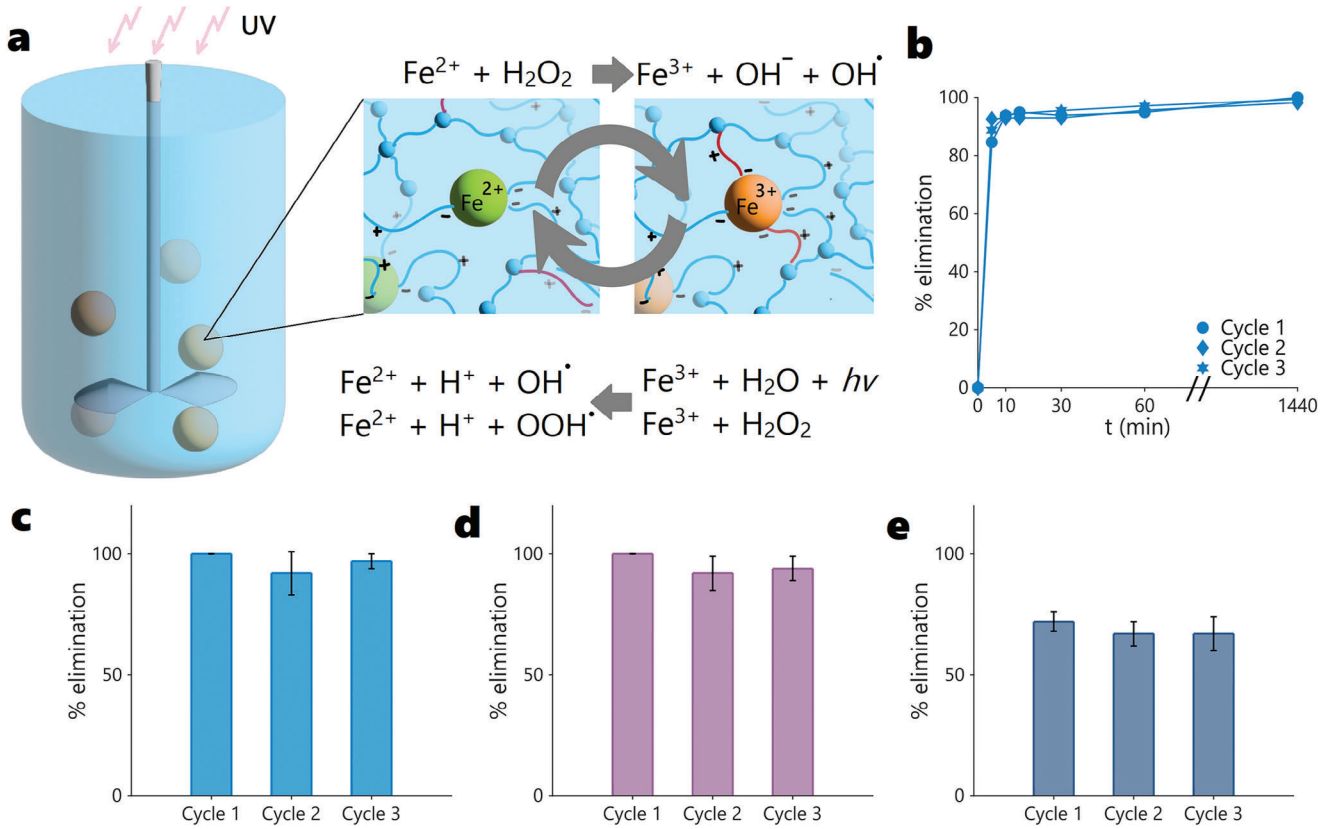

Figure 4. Regeneration and reusability of zwitterionic hydrogel catalysts. a) The simultaneous consumption and regeneration of Fe(II) ions within the hydrogel when operated in a UV–Fenton process. b) The rate of EDOL degradation over multiple cycles of use. c–e) Equilibrium elimination of c) EDOL, d) DCP, and e) PFOA, over multiple cycles of use. Error bars represent one standard deviation (n = 3).

We performed batch experiments by loading a solution of hydrogen peroxide (0.07% (w/w)) and a single POP at an environmentally relevant concentration (1 ppm) into a stirred vessel containing previously used catalytic hydrogel microparticles, to assess their ability to degrade POPs after prior use without an intervening regeneration step (see Experimental Section). As shown in Figure 4b, reusing the catalytic hydrogels in this manner in day-long batch experiments did not affect the kinetics of EDOL degradation over at least three cycles of use. Long-term testing shown in Figure S8 (Supporting Information) shows no loss in performance for EDOL degradation over 11 cycles. Similarly, when batch experiments were performed by loading fresh hydrogen peroxide and a POP into a stirred vessel containing used hydrogel microparticles every 3 h, no loss of performance was observed in elimination at the end of each 3 h cycle for all three POPs (Figure 4c–e).

3. Conclusion

We developed an innovative zwitterionic hydrogel-based heterogeneous UV–Fenton catalyst that satisfies all design requirements for a low-cost, efficient, and sustainable UV–Fenton process. Consisting of individual iron ions strongly bound to a charged and swollen hydrogel structure, our catalyst has a high effective surface area and rapid mass transport properties, allowing Fenton degradation of POPs on time scales that are within an order of magnitude of classical homogeneous Fenton reactions. Particular attention is paid to employing a scaffold material for the active iron ions that is resistant to Fenton degradation and iron loss, retains iron over time, is transparent to UV light, and can enable self-regeneration without loss in performance. Our hydrogel catalyst possesses the advantages of both, 1) prior catalysts that work at neutral pH with rapid mass transfer, and 2) prior catalysts that are heterogeneous, while suffering from the structural failure modes (ligand degradation and iron loss, respectively) and mass-transfer and other limitations of neither. The hydrogel catalyst efficiently degraded ethinyl estradiol, a xenoestrogenic endocrine disruptor, 2,4-dichlorophenol, a chlorinated pesticide of concern, and PFOA, a model for PFAS contamination. More significantly, these high levels of degradation can be achieved using a single unit operation with minimal controls. A facile and scalable synthesis, combined with high levels of POP degradation over multiple cycles of use, make the hydrogel catalyst a promising solution to urgent problems in the elimination of recalcitrant POPs from wastewater, raw water streams, and water bodies. Our hydrogel catalyst could also find use in allied areas, such as in organic synthesis or in the destruction of radioactive organic wastes.[21] Finally, similar ideas may be employed to design hydrogel-based catalysts for other advanced oxidation processes, such as those using titanium dioxide nanoparticles or other nanomaterials.

4. Experimental Section

Chemicals: N,N'-methylenebis(acrylamide) (BIS), [2-(Methacryloyloxy)ethyl]dimethyl-(3-sulfopropyl)ammonium hydroxide (PSB), poly(ethylene glycol) diacrylate (PEGDA; MW 700), 2-hydroxy-2-methylpropiophenone (PI), iminodiacetic acid (IDA), glycidyl methacrylate (GMA), ferrous sulfate heptahydrate, water (HPLC-grade), acetonitrile (HPLC-grade), methanol (HPLC-grade), formic acid (LC-MS grade; LiChropur), ammonium acetate (LC-MS grade), ethinyl estradiol (EDOL), 2,4-dichlorophenol (DCP), perfluorooctanoic acid (PFOA), mineral oil, methylene blue dye (MB), fluorescein sodium salt, ammonium persulfate, and hydrogen peroxide were purchased from Sigma–Aldrich, and used as obtained.

Synthesis of Hydrogel Microparticles: First, 5.65 g of PSB, 0.25 g of BIS, and 0.5 mL of PI (photoinitiator) were dissolved in 9.5 mL of water to produce the aqueous monomer solution (Figure 1b). This solution was processed into microparticles through an off-the-shelf microcross setup, which formed monodisperse monomer droplets of 800 ± 100 µm in diameter by pinching off the flow of monomer solution using a mineral oil phase (Figure 1a). The monomer droplets were exposed to UV light, triggering a free-radical chain-growth polymerization reaction to form hydrogel microparticles (see Figure S1, Supporting Information).

These polymerized microparticles were then washed in deionized water to remove unreacted monomers, oligomers, and residual mineral oil. The washed microparticles were subsequently soaked in saturated ferrous sulfate heptahydrate solution (1.08 M or 60% (w/w)) for 6 h to incorporate ferrous ions into the zwitterionic structure through complexation with PSB (Figure 1a). The iron-incorporated microparticles then underwent a final wash using deionized water to remove any free, excess iron ions that may still be present in the gel matrix; this prevented iron contamination of POP solutions used in degradation studies.

Methylene Blue Decomposition Experiments: In order to qualitatively determine the kinetics and efficacy of the hydrogel catalyst, test runs utilizing dilute methylene blue solutions were run in order to visually observe decomposition behavior. Six hundred milligrams of the iron-laden hydrogel was added to 5 mL of 0.05 mM (0.016 g L^{-1}) methylene blue solution and stirred continuously (Figure 2a). Then 150 µL of 1% (w/w) hydrogen peroxide solution was injected into the reaction mixture, resulting in a 0.03% (w/w) effective hydrogen peroxide concentration in the reaction mixture. No acid was added to the reaction mixture to ensure a neutral pH of approximately 7; Fenton reactions utilizing free iron required the addition of sulfuric acid, shifting the pH closer to 3, due to the precipitation of free iron at higher pH. After 10 s of mixing, the reaction mixture turned colorless, indicating fast and efficient MB decomposition by the Fenton catalyst (Figure 2a).

The reaction mixture was filmed with a OnePlus 9 smartphone camera for the duration of the reaction. Individual frames were then extracted from the video using MATLAB and an appropriate cross-section that remained stationary within the frames and did not contain hydrogel microparticles was identified. The RGB values corresponding to each pixel were converted to HSV, and the average hue within the cross-section of interest was calculated and used to track the progress of the reaction. A moving average over 0.1 s of these averaged values was reported to eliminate noise. MATLAB code used for video processing (process_vid.m) and the original videos (Videos SV1 and SV2, Supporting Information) are available in Supporting Information.

Scanning Electron Microscopy and Elemental Mapping: Samples were coated with a 5 nm Au/Pd conductive layer prior to imaging. Scanning electron microscopy images were recorded using a Zeiss Merlin High-resolution SEM with an EDX probe. Energy-dispersive X-ray spectroscopy for elemental mapping was performed at 12 kV and elemental peaks were fit using the APEX software. Maps of other elements are shown in Figure S9 (Supporting Information).

X-Ray Diffraction: A Rigaku Smartlab X-ray diffractometer equipped with a 45 kV, 200 nA, Cu Kα source (λ = 1.5406Å) was used in Bragg-Brentano geometry to analyze wet Fe ion-laden hydrogels from which free water was removed under a vacuum. Tests were performed with a scan range (2θ) of 3°–80°, a step size of 0.1°, and at a rate of 2° min^{-1}. XRD data were analyzed to obtain a pair correlation function and maximum crystallite sizes as described in Supporting Information 2.4.

Synthesis of GMA-IDA: GMA-IDA was synthesized as described previously.[72] In brief, 6.055 g IDA was dissolved in 50 mL 2M sodium hydroxide solution in water. 6.821 mL GMA was added dropwise, and the mixture was allowed to react with constant stirring in the dark at room temperature for 6 h. The reaction was confirmed using 1H-NMR spectroscopy (see Figure S10, Supporting Information). The reaction product was diluted to obtain a 0.5 M solution of GMA-IDA in water and stored in the dark at 4°C.

Synthesis of PEGDA-IDA and PSB-IDA Hydrogel Microparticles: PEGDA-IDA and PSB-IDA particles were synthesized using the previously described microfluidics setup operated in the same manner. To make PEGDA-IDA microparticles, the monomer solution was obtained by mixing 1 mL PEGDA with 8.5 mL GMA-IDA solution (prepared as previously described) and 0.5 mL PI. To make PSB-IDA microparticles, the monomer solution was obtained by dissolving 5.65 g of PSB, 0.25 g of BIS, and 0.5 mL of PI in 9.5 mL GMA-IDA solution. Microparticles obtained from the microfluidics setup were washed and soaked in iron as previously described before use.

Hydrogel Degradation and Iron Leaching: Hydrogel degradation and iron leaching was measured using 4 g hydrogel suspended in 40 mL deionized water. 3.01 mL 1% (w/w) hydrogen peroxide was then added to obtain a 0.07% (w/w) solution that was placed in a UV-enclosure for 24 h, thereby exposing the hydrogel to a UV–Fenton reaction in the absence of POP. At the end of the experiment, 3 mL of the supernatant was extracted for ICP-MS analysis to measure the amount of leached iron as described later. The remaining quantity of supernatant was measured and diluted to 80 mL and shipped to an external third-party facility (SimpleLab, USA) for TOC measurement to study hydrogel degradation. TOC measurements were performed using Standard Method SM5310 with an error of ±10%.

ICP-MS Analysis of Iron Leaching: Supernatant concentrations were measured in iron leachate samples using an inductively coupled plasma mass spectrometry (ICP-MS) (Agilent 7900 in He mode) for metals. Prior to ICP-MS analysis, samples were filtered using a 0.2 µm syringe filter, digested for 24 h in an equal volume of 70% nitric acid (to destroy organic matter), and the pH of overall mixture was subsequently increased with 75% of the equivalent amount of sodium hydroxide pellets. Finally, a volume of 200 ppb erbium solution in 4% nitric acid equal to the digested sample was added as an internal standard. In samples not containing organics, the internal standard was added as described without prior digestion in nitric acid. Linear least-squares calibrations were prepared using known standards and used to quantify iron concentrations.

Kinetics Experiments and Reuse: One gram of hydrogel catalyst was continuously stirred in a 50 mL POP solution with known initial concentration in a beaker at 500 rpm. Varying volumes of 1% (w/w) hydrogen peroxide solution in water were added to achieve the desired overall hydrogen peroxide concentration in the reaction mixture. The sample was then immediately placed in a UV-enclosure with the UV lamp on and continued stirring. A ThorLabs M365LP1 - 365 nm, 1350 mW (min), 1700 mA mounted LED at the maximum power setting was used as the UV source. Two milliliters of samples were drawn from the reaction mixture supernatant at regular intervals and stored in the dark before analysis.

As described in Section 2.2, no processing was required before the hydrogel catalyst was reused. The reaction vessel was emptied and the vessel and catalyst were washed with deionized water to remove any residual POP, fresh contaminant solution and hydrogen peroxide were added, and kinetics measurements were conducted as previously described.

Quantification of POP Concentrations: Supernatant organic micropollutant concentrations were measured using an HPLC-MS (Agilent 1100 Series LC coupled to and Agilent 6410 Triple Quadrupole MS), adapting a previously described method.[19,73] The triple quadrupole MS was operated in full scan mode to detect ions with a mass-to-charge ratio in the range 100 to 1000, and chromatograms corresponding to the micropollutants of interest were extracted during post-processing. The limit of detection of each micropollutant was the lowest concentration at which the height of the peak corresponding to that micropollutant was twice the background level.

EDOL was analyzed in positive polarization mode, and samples were injected in 100 µ L volumes into an Kinetex (Phenomenex Inc.) C18 column (particle size 2.6 µ m, pore size 100 Å, 100 × 4.6 mm) using a gradient pump delivering 300 µ L min^{-1} of a water and methanol mobile phase, each containing 0.1% formic acid. The gradient, retention times, and linear least-squares calibration curves were developed using known standards, and are described in Supporting Information 2.5.

DCP and PFOA-containing samples were analyzed in negative polarization mode, and injected in 50 µ L volumes into a Zorbax eclipse XDB (Agilent Technologies) C18 column (particle size 3.5 µ m, pore size 80 Å, 100 × 2.1 mm). For DCP quantification, the process was operated in isocratic mode with a pump delivering 500 µ L min^{-1} of a 60% methanol/40% water buffer. For PFOA quantification, a gradient pump was used for delivering 150 µ L min^{-1} of a 0.2 g L^{-1} ammonium acetate in water, and 100% acetonitrile mobile phase. The gradient, retention times, and linear least-squares calibration curves were developed using known standards, and are described in Supporting Information 2.5.

Supporting Information

Supporting Information is available from the Wiley Online Library or from the author.

Acknowledgements

D.G. and I.C. contributed equally to this work. This work was funded by the MIT Abdul Latif Jameel Water and Food Systems Lab (J-WAFS). D.G. also thanks the Rasikbhai L. Meswani Fellowship for Water Solutions and the Raj V. Tahil (1981) Fellowship Fund Award for funding. I.C. also thanks MIT UROP (Undergraduate Research Opportunities Program) for funding. W.-N.W. thanks MIT Nano, the MIT Materials Research Laboratory (MRL), and Prof. Z. Smith for the use of experimental facilities. D.G. thanks the MIT Center for Environmental and Health Sciences (CEHS), J.D.J. Rathinaraj and Prof. G.H. McKinley, and G. Getzinger and Prof. J. Kroll for the use of experimental facilities.

Conflict of Interest

The authors declare no conflict of interest.

Data Availability Statement

The data that support the findings of this study are available from the corresponding author upon reasonable request.

Keywords

fenton oxidation, hydrogels, water treatment

Received: April 19, 2024
Revised: May 7, 2024
Published online: May 27, 2024

[1] R. P. Schwarzenbach, B. I. Escher, K. Fenner, T. B. Hofstetter, C. A. Johnson, U. von Gunten, B. Wehrli, *Science* **2006**, *313*, 1072.
[2] S. D. Richardson, T. A. Ternes, *Anal. Chem.* **2014**, *86*, 2813.
[3] S. T. Glassmeyer, E. T. Furlong, D. W. Kolpin, A. L. Batt, R. Benson, J. S. Boone, O. Connerly, M. J. Donohue, D. N. King, M. S. Kostich, H. E. Mash, S. L. Pfaller, K. M. Schenck, J. E. Simmons, E. A. Varughese, S. J. Vesper, E. N. Villegas, V. S. Wilson, *Sci. Total Environ.* **2017**, *581–582*, 909.
[4] D. W. Kolpin, E. T. Furlong, M. T. Meyer, E. M. Thurman, S. D. Zaugg, L. B. Barber, H. T. Buxton, *Environ. Sci. Technol.* **2002**, *36*, 1202.
[5] S. Jobling, M. Nolan, C. R. Tyler, G. Brighty, J. P. Sumpter, *Environ. Sci. Technol.* **1998**, *32*, 2498.
[6] P. Matthiessen, P. E. Gibbs, *Environ. Toxicol. Chem.* **2009**, *17*, 37.
[7] K. Steenland, T. Fletcher, D. A. Savitz, *Environ. Health Perspect.* **2010**, *118*, 1100.
[8] F. Acconcia, V. Pallottini, M. Marino, *Dose–Response* **2015**, *13*, 1.
[9] K. E. Murray, S. M. Thomas, A. A. Bodour, *Environ. Pollut.* **2010**, *158*, 3462.
[10] C. G. Daughton, T. A. Ternes, *Environ. Health Perspect.* **1999**, *107*, 907.
[11] F. M. M. Morell, A. M. L. Kraepiel, M. Amyot, *Exotoxicol. Environ. Saf.* **1998**, *29*, 543.
[12] R. van der Oost, J. Beyer, N. P. E. Vermeulen, *Exotoxicol. Toxicol. Pharmacol.* **2003**, *13*, 57.
[13] Y. Vasseghian, S. Hosseinzadeh, A. Khataee, E.-N. Dragoi, *Sci. Total Environ.* **2021**, *796*, 149000.
[14] Z. Wang, S. Adu-Kumi, M. L. Diamond, R. Guardans, T. Harne, A. Harte, N. Kajiwara, J. Klanova, J. Liu, E. G. Moreira, D. C. G. Muir, N. Suzuki, V. Pinas, T. Seppala, R. Weber, B. Yuan, *Environ. Sci. Technol.* **2022**, *56*, 2936.
[15] E. I. du Pont de Nemours and Company, $DuPont_{TM}$ GenX Processing Aid for Making Fluoropolymer Resins: Setting a New Industry Standard for Sustainable Replacement Technology, https://api1.ibabs.eu/publicdownload.aspx?site=sliedrecht&id=100013871, (accessed: October 2023).
[16] United States Environmental Protection Agency (USEPA), PFAS Strategic Roadmap: EPA's Commitments to Action 2021-2024, https://www.epa.gov/system/files/documents/2021-10/pfas-roadmap_final-508.pdf, (accessed: October 2023).
[17] European Chemicals Agency (ECHA), ECHA publishes PFAS restriction proposal, https://echa.europa.eu/-/echa-publishes-pfas-restriction-proposal, (accessed: October 2023).
[18] United Nations Organization, United nations sustainable goals - goal 6, **2004**, https://sdgs.un.org/goals/goal6.
[19] D. Gokhale, A. F. Hamelberg, P. S. Doyle, *Nat. Water* **2024**, *2*, 62.
[20] H. J. H. Fenton, *J. Chem. Soc. Trans.* **1894**, *65*, 899.
[21] S. A. Walling, W. Um, C. L. Corkhill, N. C. Hyatt, *npj Mater. Degrad.* **2021**, *5*, 50.
[22] H. Tang, Q. Xiang, M. Lei, J. Yan, L. Zhu, J. Zou, *Chem. Eng. J.* **2012**, *184*, 156.
[23] A. D. Bokare, W. Choi, *J. Hazard. Mater.* **2014**, *275*, 121.
[24] S. R. Pouran, A. A. A. Raman, W. M. A. W. Daud, *J. Clean. Prod.* **2014**, *275*, 121.
[25] A. Babuponnusami, K. Muthukumar, *J. Environ. Chem. Eng.* **2014**, *2*, 557.
[26] M. I. Litter, M. Slodowicz, *J. Adv. Oxid. Technol.* **2017**, *20*, 20160164.
[27] R. C. Martins, L. R. Henriques, R. M. Quinta-Ferreira, *Chem. Eng. Sci.* **2013**, *100*, 225.
[28] M. E. Farshchi, H. Aghdasinia, A. Khataee, *J. Clean. Prod.* **2018**, *182*, 644.
[29] F. Liu, J. Li, *Earth Environ. Sci.* **2018**, *146*, 012023.
[30] M. Xu, C. Wu, Y. Zhou, *Advanced Oxidation Processes*, chapter 4: Advancements in the Fenton Process for Wastewater Treatment, IntechOpen, **2020**.
[31] G.-M. Cao, M. Sheng, W.-F. Niu, Y.-L. Fei, D. Li, *J. Hazard. Mater.* **2009**, *2–3*, 1446.
[32] H. Zhang, J. Liu, C. Ou, Faheem, J. Shen, H. Yu, Z. Jiao, W. Han, X. Sun, J. Li, L. Wang, *J. Environ. Sci.* **2017**, *53*, 1.
[33] E. Brillas, S. Garcia-Segura, *Sep. Purif. Technol.* **2020**, *237*, 116337.
[34] C. S. D. Rodrigues, O. S. G. P. Saares, M. F. R. Pereira, L. M. Madeira, *J. Water Process Eng.* **2021**, *44*, 102386.
[35] P. Compton, N. R. Dekhordi, P. L. Casanova, A. N. Alshawabkeh, *J. Chem. Eng. Catal.* **2022**, *1*, 203.

[36] X. Wang, X. Zhang, Y. Zhang, Y. Wang, S.-P. Sun, W. D. Wu, Z. Wu, *J. Mater. Chem. A* **2020**, *8*, 15513.
[37] M. Arshadi, M. K. Abdolmaleki, F. Mousavinia, A. Khalafi-Nezhad, H. Firouzabadi, A. Gil, *Chem. Eng. Res. Des.* **2016**, *112*, 113.
[38] Q. Z. Huang, S. M. Wang, J. F. Huang, L. H. Zhuo, Y. C. Guo, *Carbohydr. Polym.* **2007**, *68*, 761.
[39] C. J. Miller, A. L. Rose, T. D. Waite, *Front. Mar. Sci.* **2016**, *3*, 134.
[40] G. Farinelli, M. Minella, M. Pazzi, S. Giannakis, C. Pulgarin, D. Vione, A. Tiraferri, *J. Hazard. Mater.* **2020**, *393*, 122413.
[41] A. Fischbacher, C. von Sonntag, T. C. Schmidt, *Chemosphere* **2017**, *182*, 738.
[42] F. Haber, J. Weiss, *Proc. Roy. Soc. A* **1934**, *147*, 332.
[43] A. D. Luca, R. F. Dantas, S. Esplugas, *Water Res.* **2014**, *61*, 232.
[44] K. Hislop, J. R. Bolton, *Environ. Sci. Technol.* **1999**, *33*, 3119.
[45] J. A. Giroto, A. C. Teixeira, C. A. Nascimento, R. Guardani, *Ind. Eng. Chem. Res.* **2010**, *49*, 3200.
[46] J. A. Giroto, R. Guardani, A. C. S. Teixeira, C. A. O. d. Nascimento, *Chem. Eng. Process.: Process Intensif.* **2006**, *45*, 523.
[47] G. Ruppert, R. Bauer, G. Heisler, *J. Photochem. Photobiol. A: Chem.* **1993**, *73*, 75.
[48] United States Environmental Protection Agency, Drinking water contaminant candidate list (ccl) and regulatory determination, https://www.epa.gov/ccl, (accessed: January 2023).
[49] A. Erfani, P. Zarrintaj, J. Seaberg, J. D. Ramsey, C. P. Aichele, *J. Appl. Polym. Sci.* **2021**, *138*, 50545.
[50] X. Zhou, Y. Guo, F. Zhao, G. Yu, *Acc. Chem. Res.* **2019**, *52*, 3244.
[51] V. Sinha, S. Chakma, *J. Environ. Chem. Eng.* **2019**, *7*, 103295.
[52] D. Gokhale, I. Chen, P. S. Doyle, *ACS Appl. Polym. Mater.* **2022**, *4*, 746.
[53] E. Amstad, M. Chemama, M. Eggersdorfer, L. R. Arriaga, M. P. Brenner, D. A. Weitz, *Lab Chip* **2016**, *21*, 20.
[54] TU Graz, Atomic form factors, https://lampx.tugraz.at/~hadley/ss1/crystaldiffraction/atomicformfactors/formfactors.php (accessed: October 2023).
[55] Q. Wang, S. Tian, P. Ning, *Ind. Eng. Chem. Res.* **2014**, *53*, 643.
[56] K. Dutta, S. Mukhopadhyay, S. Bhattacharjee, B. Chaudhuri, *J. Hazard. Mater.* **2001**, *84*, 57.
[57] Y. Ahmed, Z. Yaakob, P. Akhtar, *Catal. Sci. Technol.* **2016**, *6*, 1222.
[58] H. G. Quynh, H. V. Thanh, N. T. T. Phuong, N. P. T. Duy, L. H. Hung, N. V. Dung, N. T. H. Duong, N. Q. Long, *Environ. Technol. Inno.* **2023**, *31*, 103155.
[59] G. Farinelli, S. Giannakis, A. Schaub, M. Kohantorabi, C. Pulgarin, *Water Res.* **2024**, *255*, 121518.
[60] United States Environmental Protection Agency, National primary drinking water regulations, https://www.epa.gov/sites/default/files/2016-06/documents/npwdr_complete_table.pdf (accessed: February 2023).
[61] J. Nakrst, M. Bistan, T. Tisler, J. Zagorc-Koncan, J. Derco, A. Z. Gotvajn, *Water Sci. Technol.* **2011**, *63*, 2131.
[62] H. Wang, Y. Zhao, Y. Su, T. Li, M. Yao, C. Qin, *RSC Adv.* **2017**, *7*, 4563.
[63] D. R. Schlesinger, C. McDermott, N. Q. Le, J. S. Ko, J. K. Johnson, P. A. Demirev, Z. Xia, *Environ. Sci.: Water Res. Technol.* **2022**, *8*, 2732.
[64] J. Ma, W. Song, C. Chen, W. Ma, J. Zhao, Y. Tang, *Environ. Sci. Technol.* **2005**, *39*, 5810.
[65] S. Ferhi, J. Vieillard, C. Garau, O. Poultier, L. Demey, R. Beaulieu, P. Penalva, V. Gobert, F. Portet-Koltalo, *J. Environ. Chem. Eng.* **2021**, *9*, 106120.
[66] J. Liu, Y. Du, W. Sun, Q. Chang, C. Peng, *RSC Adv.* **2019**, *9*, 22513.
[67] C. Wang, R. Jiang, J. Yang, P. Wang, *Front. Chem.* **2022**, *10*, 892424.
[68] L. Shi, Y. Zhang, C. Zeng, X. Lai, S. Chen, *J. Clean. Prod.* **2022**, *376*, 134259.
[69] M. Rodriguez, N. B. Abdrerrazik, S. Contreras, E. Chamarro, J. Gimenez, S. Esplugas, *Appl. Catal. B: Environ.* **2002**, *37*, 131.
[70] H. Kusic, N. Koprivanac, I. Selanec, *Chemosphere* **2006**, *65*, 65.
[71] J. Feng, S. Li, Y. Sheng, Y. Xiong, S. Lan, S. Tian, L. Kong, C. Fan, *Appl. Catal. A: Gen.* **2024**, *542*, 21.
[72] A. J. Macbeth, Z. Lin, J. M. Goddard, *MethodsX* **2020**, *7*, 101110.
[73] S. Huntscha, H. P. Singer, C. S. McArdell, C. E. Frank, J. Hollender, *J. Chromatogr. A* **2012**, *1268*, 74.